A Multistate Empirical Valence Bond Description of Protonatable Amino Acids †

5 **AUTHORS**, INCLUDING:

Christopher Maupin
Colorado School of Mines
35 PUBLICATIONS **580** CITATIONS

Alexander V. Soudackov
University of Illinois, Urbana-Champaign
54 PUBLICATIONS **1,753** CITATIONS

A Multistate Empirical Valence Bond Description of Protonatable Amino Acids[†]

C. Mark Maupin, Kim F. Wong, Alexander V. Soudackov,[‡] Sun Kim,[§] and Gregory A. Voth*

Center for Biophysical Modeling and Simulation and the Department of Chemistry, University of Utah, Salt Lake City, Utah 84112-0850

The multistate empirical valence bond (MS-EVB) model, which was developed for molecular dynamics simulations of proton transport in water and biomolecular systems, is extended for the modeling of protonatable amino acid residues in aqueous environments, specifically histidine and glutamic acid. The parameters of the MS-EVB force field are first determined to reproduce the geometries and energetics of the gas phase amino acid−water clusters. These parameters are then optimized to reproduce experimental pK_a values. The free energy profiles for acid ionization and the corresponding pK_a values are calculated by MS-EVB molecular dynamics simulations utilizing the umbrella sampling technique, with the center of excess charge coordinate chosen as the dissociation reaction coordinate. A general procedure for fitting the MS-EVB parameters is formulated, which allows for the parametrization of other amino acid residues with protonatable groups and the subsequent use of the MS-EVB approach for molecular dynamics simulations of proton transfer processes in proteins involving protonation/deprotonation of the protonatable amino acid groups.

1. Introduction

The protonation state of amino acid residues plays a key role in determining protein conformational mobility, enzyme catalysis, substrate binding, and proton translocation pathways.[1−17] One of the most intensively studied proton transport (PT) processes in enzymes occurs in carbonic anhydrase (CA) during the interconversion of carbon dioxide and bicarbonate. The rate-limiting step for this reaction is one of two PT events, the PT from the zinc bound water through a water bridge to His64[6] or the PT from His64 to bulk water,[10] depending on the exogenous buffer concentration. Site-directed mutations of the acidic residue at position 64 in human carbonic anhydrase (HCA) to nonionizable residues (H64A and L64E) leads to a reduction in the enzymatic activity of 10−50-fold.[9,18] Buffering the H64A mutant in a solution of 4-methyl-imidazole, a molecule with an acid proton, recovered as much as 40% of the maximal activity observed in the wild-type system.[19,20] Such *chemical rescue* of enzymatic activity suggests a direct link between the chemical nature of the protein residue and the enzyme activity. In addition to affecting catalysis, the protonation state of amino acids also affects proton diffusion through the influenza A virus M2 ion channel.[2,3] In the M2 ion channel a set of four histidines form the entrance of the channel and are responsible for the experimentally observed gating mechanism via a reversible protonation/deprotonation of the histidine residues. To describe the PT processes, a model that accurately describes the ability of ionizable residues to act as a proton acceptor/donor is of key importance. However, and more importantly, the model must also incorporate the process of *proton shuttling* of the excess proton away from the conjugate base via the Grotthuss mechanism.[21,22]

While the aforementioned systems illustrate the importance of ionizable amino acid residues in biological systems, conventional molecular dynamics (MD) simulations do not permit explicit protonation/deprotonation dynamics or Grotthuss shuttling during the trajectory. In a typical protein simulation, the protonation states of the constituent residues are initially determined and remain a constant for the remainder of the simulation. This approach is inadequate when the conformational sampling is sensitive to the protonation states and when the protonation states may change in response to the sampled configurations. This deficiency in molecular dynamics becomes evident when attempting to calculate pK_a values for ionizable amino acid residues in biological systems.

When the pK_a value of a solvent-exposed amino acid residue is comparable to the pH of the aqueous buffer solution, the deproation process can be described by the general weak acid equilibrium dissociation reaction

$$HA + H_2O \leftrightarrow A^- + H_3O^+ \tag{1}$$

where the acid HA donates a proton to water to form the conjugate base A^- and a hydronium H_3O^+. Methodologies that are based on standard classical molecular mechanical force fields with fixed molecular bonding topologies are not adequate to treat such reactions, as bond cleavage and formation are the essential part of the chemistry. One implementation that can describe chemical dynamics at a computational expense similar to MD is the empirical valence bond (EVB) approach.[1] In the simplest two-state case, the system is described by the ground state potential energy surface of a 2×2 Hamiltonian matrix, where the diagonal elements are the valence bond states describing the reactant and the product and the off-diagonal element (coupling) contains all the physics for describing the transitions between reactant and product wells. Typically the diagonal elements are computed at the level of classical mechanical force fields, and the off-diagonal element is

---

* Corresponding author. E-mail: voth@chem.utah.edu.
[‡] Current address: Department of Chemistry, The Pennsylvania State University, University Park, PA 16802.
[§] Current address: Department of Chemistry, University of California, Berkeley, CA 94720.

parametrized to reproduce experimental properties or results from quantum mechanical calculations on small fragments of the system.

The multistate empirical valence bond (MS-EVB) model for PT in water[23−26] is a model capable of handling transient molecular topologies and recently has been extended for the description of weak acid (WA) dissociation processes in water.[27,28] In the latter augmented MS-EVB model, an additional EVB state describing the protonated acid molecule is explicitly included within the MS-EVB description of PT in water. Thus in the reaction system consisting of a WA surrounded by water molecules there are two classes of EVB states (although there may be many EVB states in number). The first class corresponds to the protonated acid molecule HA and the second corresponds to the hydronium (H_3O^+) ion from eq 1, where the WA and water are strongly coupled during the initial PT event.

The present paper describes the development of a general and systematic MS-EVB parametrization procedure and its application to histidine and glutamic acid, two of the relatively few protonatable amino acid residues found in proteins. Utilizing WA models that accurately describe the protonation event will allow for the study of a multitude of biological environments with several different amino acid residues. These WA models will allow for detailed analysis of the related mechanistic and dynamical properties of proteins, which can help to explain pH-dependent experimental results. This approach also promises to provide a better understanding of the role amino acids play in PT in proteins.

2. Methodology

The MS-EVB method for simulating proton transport in aqueous solution and the generalization to acid dissociation reactions have been presented in full detail elsewhere.[23−26] The present study describes modifications to the previous methodology and provides a more systematic procedure for obtaining the parameters for ionizable amino acid residues. In this section, we briefly summarize the MS-EVB approach for treating proton transport, outline the optimization scheme for determining MS-EVB parameters for amino acid residues, and describe the simulation details to our implementation for histidine and glutamic acid.

A. MS-EVB Potential. In the MS-EVB model, the system evolves on the potential energy surface that is defined as the lowest energy solution of the Hamiltonian matrix in the representation of valence bond states $|i(\mathbf{r})\rangle$

$$\mathbf{H}^{EVB} = \sum_{ij} |i(\mathbf{r})\rangle h_{ij}(\mathbf{r})\langle j(\mathbf{r})| \qquad (2)$$

where the vector $\mathbf{r}$ represents the complete set of nuclear degrees of freedom. The diagonal elements of the EVB Hamiltonian h_{ii} correspond to the potential energy of EVB state $|i\rangle$, and the off-diagonal elements h_{ij} represent the coupling between EVB states $|i\rangle$ and $|j\rangle$.

The algorithm used for generating the set of EVB states during the MD is based on the implementation described in the second generation MS-EVB paper.[26] As an example, Figure 1 depicts the complete set of valence bond states for a system composed of a histidine amino acid residue, an excess proton, and three water molecules. In EVB state 1, the proton is bonded to the nitrogen of the imidazole moiety of the histidine side chain, whereas in EVB state 2, the proton is bonded to the oxygen of a nearby water. Permutation of the excess proton bonding topology between the other two waters defines EVB
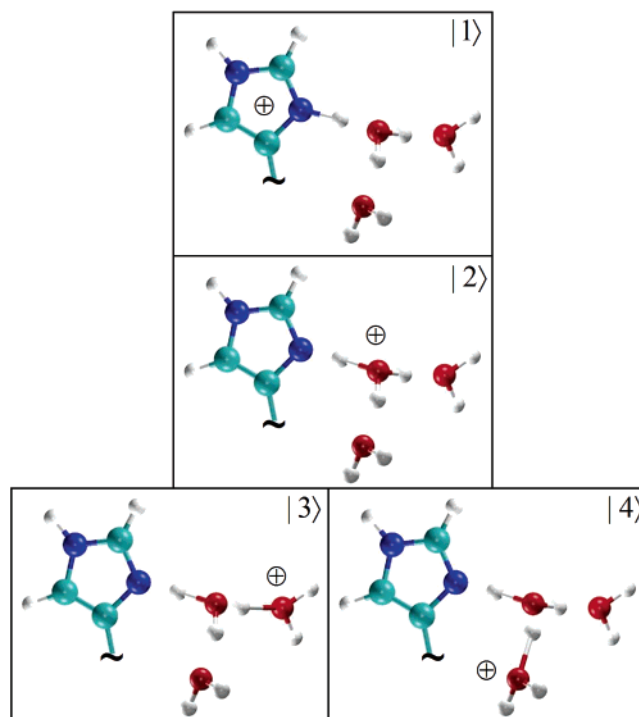

Figure 1. Schematic picture of the HisH$^+$−(H$_2$O)$_3$ ($|1\rangle$) and His−H$_3$O$^+$−(H$_2$O)$_2$ ($|2\rangle$, $|3\rangle$, and $|4\rangle$)) diagonal EVB states used in the MS-EVB model.

states 3 and 4. One can imagine that the number of EVB states can grow exponentially as the number of solvating waters approaches the bulk limit. Since the couplings between a donor EVB state and the acceptor EVB states are expected to decay as a function of distance, the EVB state generation routine truncates the basis set based on solvation distance criteria. It has been shown that a general cutoff criterion of 2−3 solvation shells is sufficient for most applications, although this parameter can be adjusted to satisfy the level of accuracy and computational practicality that one desires. The ability of the MS-EVB method to treat many EVB states in the underlying solvent and thus its ability to include the important Grotthuss shuttling behavior in the acid dissociation distinguish the MS-EVB method from the earlier and simpler EVB approach.[1]

The potential energy corresponding to each of the above EVB state molecular topologies is computed using the AMBER[29] force field, which has been shown to be adequate in describing equilibrium structures, conformational energies, and interaction energies of proteins, nucleic acids, and related organic molecules. The interactions that comprise h_{ii} include terms describing bond stretches, angle bends, proper and improper dihedral bends, Lennard-Jones interactions, and electrostatics. To properly represent the dissociation limit as a proton transfers from the donor to the acceptor, we replace the AMBER[29] harmonic bond stretch potential describing the donor−proton bond and the acceptor−proton bond vibrations with a standard Morse function,

$$U^{Morse}(r) = a_0[1 - e^{a_1(r-a_2)}]^2 \qquad (3)$$

where a_0, a_1, and a_2 are parameters. These parameters were determined by fitting the gas phase ab initio relaxed potential energy scan for the deprotonation reaction of the bare amino acid residue (no solvating water cluster) to the above functional form. Since systems with differing molecular topologies do not share a common (classical force field) energy origin, each

MS-EVB Description of Protonatable Amino Acids

J. Phys. Chem. A, Vol. 110, No. 2, 2006 **633**

diagonal EVB matrix element is augmented with a constant energy shift parameter V_{ii}^0 to correct for the relative energies among the EVB states.

The off-diagonal elements of the EVB matrix contain all the interactions responsible for describing transitions among the empirically determined EVB states and are represented by the functional form

$$h_{ij}(q, R_{DA}) = V_{ij}^{const} f(R_{DA}) \, g(q) \tag{4}$$

where q is the PT coordinate, R_{DA} is the distance between the donor D and acceptor A atoms, and V_{ij}^{const} is an adjustable parameter. The functions $f(R_{DA})$ and $g(q)$ are defined as

$$f(R_{DA}) = [C \exp\{-\alpha(R_{DA} - a_{DA})^2\} + (1 - C)$$
$$\exp\{-\beta(R_{DA} - b_{DA})^2\}][1 + \tanh\{\epsilon(R_{DA} - c_{DA})\}] \tag{5}$$

$$g(q) = \exp[-\gamma q^2] \tag{6}$$

where C, α, β, γ, ϵ, a_{DA}, b_{DA}, and c_{DA} are adjustable parameters. The PT coordinate q is defined in terms of the distance between the proton H^+ and a point on the line connecting the donor and acceptor atoms,

$$q = |\mathbf{R}_{DH^+} - r_{sc}\frac{\mathbf{R}_{DH^+}}{2}| \tag{7}$$

where

$$r_{sc} = r_{sc}^0 - \lambda(R_{DA} - R_{DA}^0) \tag{8}$$

and r_{sc}^0, λ, and R_{DA}^0 are also adjustable parameters. The combination of the AMBER[29] force field (with the modifications noted earlier) and the functional form for the coupling element and the associated parameters constitutes the MS-EVB force field for PT in aqueous amino acid systems.

B. MS-EVB Parametrization. The MS-EVB parameters for a particular amino acid residue were determined in two stages: an initial parametrization to fit results from quantum mechanical (QM) calculations followed by a parametrization to reproduce experimental solution pK_a values. While empirical potentials can adequately represent the dynamics of stable EVB states, they cannot describe transitions over the barriers between these states. Quantum chemistry has matured to the point where it has now become computationally practical to elucidate properties of transition states or map out the potential energy surface (PES) for a moderate size system at a reasonably accurate level of theory. An amino acid model in an aqueous phase or inside a protein environment, however, remains computationally expensive for direct calculation using quantum chemistry methodologies.

Our approach is to first fit the MS-EVB parameters to reproduce the ab initio PT PES along with the geometric features of small amino acid−water clusters in the gas phase. Since the PT barrier height depends strongly on the donor−acceptor distance R_{DA}, the PT PES includes this degree of freedom in addition to the donor−proton distance R_{DH^+}. The geometries of the amino acid−water clusters were optimized at the level of density function theory (DFT) using the B3LYP/6-31G(d,p) functional/basis set. During the optimization, all of the coordinates are allowed to relax except for the constraints imposed on the R_{DA} and R_{DH^+} bond lengths. The nonlinear dependence of the MS-EVB electronic ground state energy on the coupling parameters precludes a direct solution of these parameters, i.e., by matrix factorization methods. A nonunique set of parameters,

however, can be determined using an iterative procedure. Starting from an initial guess of the MS-EVB parameters, a subspace searching variant of the Simplex[30] optimization method was employed to minimize the sum of square deviations between the MS-EVB PT PES and the ab initio PES. The sum of square deviations of the MS-EVB derived equilibrium R_{DA} and R_{DH^+} distances and $\angle_{DH^+A}$ angle relative to the geometric properties obtained from the ab initio calculations was also included in the target function. Optimization of this target function provides a preliminary set of parameters.

In general, these optimized parameters from gas phase clusters do not provide an adequate description of the solution phase dissociation reaction and need to be adjusted to reproduce experimental pK_a values. If one were to use the set of MS-EVB parameters that were optimized for the system depicted in Figure 1 to simulate the deprotonation of histidine inside a periodic cell containing 500 water molecules, it would not be surprising if the equilibrium concentrations for the reactants and products do not agree with experimental measurements. However, the primary effect of adding more solvating waters is to change the relative free energies of the EVB state minima, thus altering the direction of the equilibrium. The V_{ii}^0 parameter in the diagonal element of the EVB matrix adjusts the energy difference between the HisH$^+$ EVB state and the H$_3$O$^+$ EVB state of Figure 1 to correctly reproduce the asymmetry of the ab initio PES about the barrier. Since the gas phase cluster includes only a limited number of solvent molecules, the optimized parameters from such a model are generally not transferable to simulations consisting of bulk solvent densities. An indication of this lack of transferability is the disagreement between the simulation derived pK_a value and experiment.

One strategy for refining the preliminary MS-EVB parameters so that they can be used in condensed phase simulations is to constrain all parameters except for the V_{ii}^0 term and adjust this value until the amino acid in bulk water simulation reproduces the experimental pK_a. Each pK_a calculation, using the procedure described below, requires the generation of a new potential of mean force (PMF). Altering the value of the V_{ii}^0 parameter to fit solution chemistry invariably reduces the agreement between the MS-EVB and ab initio gas phase cluster potential energy surfaces. An alternative, computationally more demanding, strategy is to self-consistently optimize the MS-EVB parameters for both the gas phase and condensed phase systems until one arrives at a single parameter set that is practical for both types of simulations. One cycle of the iterative procedure consists of the following steps: (1) optimize the MS-EVB parameters to reproduce results from QM calculations on the cluster system, (2) constrain all parameters except for V_{ii}^0 and adjust this constant energy offset so that the condensed phase simulations using this modified parameter set reproduce the experimental pK_a, and (3) return to the first step and optimize all the parameters except for V_{ii}^0. The last step corrects the parameters to compensate for the effect on the MS-EVB PES from changing the previously optimized (gas phase) V_{ii}^0 parameter. To explore both alternatives (neither of which is perfect), the first approach was used for the parametrization of histidine, while the iterative procedure was used for the parametrization of glutamic acid.

The calculation of the pK_a is based on the classical statistical mechanics expression[31]

$$pK_a = \log[4\pi \int_0^{\ddagger} d\xi \, \xi^2 \, e^{-\beta G(\xi)}] \tag{9}$$

where $\beta = 1/(k_B T)$ is the inverse of the Boltzmann factor, $G(\xi)$ is the free energy (potential of mean force) as a function of the

634 *J. Phys. Chem. A, Vol. 110, No. 2, 2006*

Maupin et al.

reaction coordinate (RC) ξ, and $\ddagger$ is the value of the RC dividing the reactants (protonated amino acid and water) from the products (deprotonated amino acid and a solvated hydronium). An outline of the derivation is provided as Supporting Information.

The free energy barrier separating the protonated and deprotonated states is typically much larger than the accessible thermal energy at standard temperature. To enhance the sampling of rare events near the transition state region, we use umbrella sampling[32,33] and adaptive sampling techniques.[34] The dissociation RC ξ_{CEC} was defined as the distance between the center of excess charge (CEC) of the MS-EVB complex and the amino acid donor atom $\mathbf{r}_D$

$$\xi_{CEC} = |\mathbf{r}_{CEC} - \mathbf{r}_D| \qquad (10)$$

where $\mathbf{r}_{CEC}$ is the center of excess protonic charge defined as

$$\mathbf{r}_{CEC} = \sum_i^{N_{EVB}} c_i^2(\mathbf{r})\mathbf{r}_i^{COC} \qquad (11)$$

In the above equation, N_{EVB} is the total number of EVB states, $c_i^2(\mathbf{r})$ is the population of EVB state i contributing to the MS-EVB ground state, and $\mathbf{r}_i^{COC}$ is the position of the center of charge given by

$$\mathbf{r}_i^{COC} = \frac{1}{\sum_k^{\{i\}} |q_k|} \sum_k^{\{i\}} |q_k|\mathbf{r}_k \qquad (12)$$

where the summations are over the atoms (with partial charge q_k) comprising the ith EVB complex. A series of harmonic restraining potentials

$$U_n^{umbrella}(\xi_{CEC}) = \frac{k_n}{2}(\xi_{CEC} - \xi_0^n)^2 \qquad (13)$$

were used to bias the sampling of ξ_{CEC}, spanning from the protonated amino acid out to the bulk aqueous phase. The force constants k_n were adjusted to ensure adequate sampling in each window, and the restraint points ξ_0^n were chosen to give sufficient overlap between adjacent windows. The constant temperature weighted histogram analysis method[35,36] (WHAM) was used to unbias the individual umbrella simulations for constructing the PMF corresponding to dynamics on the EVB ground state. In the adaptive sampling approach the phase space sampling is enhanced by adding the negative of the PMF to the Hamiltonian. This procedure effectively removes the free energy barrier, and the sampling becomes uniform along the RC.

C. Simulation Details for Histidine. The histidine model for the gas phase small cluster calculations consists of an all-atom representation of the protonated (zwitterionic) histidine and three solvating waters adjacent to the N_δ nitrogen atom of the imidazole ring. Standard AMBER[29] capping groups Ace and Nme terminate the N- and C-terminus of the amino acid residue. Since the PT barrier height depends strongly on the donor–acceptor distance, six different fixed $R_{N_\delta O}$ distances of 2.4, 2.5, 2.6, 2.7, 2.8, and 2.9 Å were used as the transferring hydrogen atom was scanned in increments of 0.05 Å from the donor histidine to the nearest acceptor water. The geometry of the HisH$^+$–(H$_2$O)$_3$ cluster was optimized at the level of DFT using the B3LYP/6-31G(d,p) functional/basis set. During the optimization, all degrees of freedom were relaxed except for the

independent variables of the PES (the $R_{N_\delta O}$ and $R_{N_\delta H^+}$ distances). The equilibrium bond lengths ($R_{N_\delta O}$ and $R_{N_\delta H^+}$) and equilibrium bond angle ($\angle_{N_\delta H^+ O}$) were also computed at the same level of accuracy. All of the above ab initio calculations were performed with the *Gaussian 03* program package.[37] Using a subspace searching version of the Simplex[30] algorithm, we fit the MS-EVB parameters to the QM data by minimizing the sum of square deviations between the corresponding MS-EVB PT PES and equilibrium geometrical properties relative to the ab initio counterparts. The MS-EVB calculations were performed using a modified DL_POLY 2.14 software[38] incorporating the MS-EVB algorithm.[39] These optimized parameters were then used in subsequent aqueous phase simulations to compute the pK_a value described below.

The solution phase histidine model consists of the above Ace/Nme-terminated histidine residue immersed in a cubic simulation box ($L = 19.66$ Å) containing 241 modified TIP3P water molecules and one chloride counterion. With the exception of using a Morse potential to describe the gas phase dissociation limit of the histidine $N_\delta H^+$ bond, the AMBER[29] force field was used to describe the amino acid model and the counterion. The fitting of the Morse function to the gas phase deprotonation potential energy profile yielded the following parameters: $a_0 = 135.07$ kcal/mol, $a_1 = -2.06$ Å^{-1}, and $a_2 = 1.01$ Å. Periodic boundary conditions were employed, and the long-range Coulombic interactions were treated with Ewald summation.[40] The short-range nonbonded interactions and forces were subject to a 9.5 Å cutoff. The MD time integration step within the Verlet integrator was 0.5 fs in all simulations. As in the imidazole MS-EVB parametrization,[27] to compensate for an overattraction between the histidine's N_δ proton donor/acceptor atom and the hydronium hydrogens, a Lennard-Jones potential was used to describe the interaction between the excess proton and the histidine atoms, with the proton's LJ parameters being $\sigma = 0.40$ Å and $\epsilon = 0.046$ kcal/mol. Prior to the MS-EVB simulations, the above classical system was equilibrated for 1 ns in the constant NVE ensemble followed by an additional 2 ns of equilibration in the constant NPT ensemble.[41]

For the calculation of the pK_a, one needs to generate the PMF for proton dissociation into the bulk. A total of 80 umbrella windows, spanning the range of $\xi_0^n = 0.65$ to 4.45 Å, were used to enhance sampling of phase space. The umbrella force constant, k_n, was varied from 175 to 450 kcal mol^{-1} Å^{-2}. Each window was equilibrated in the constant NVT ensemble[41] using a Nose-Hoover thermostat for 25 ps followed by data collection for a period of 100 ps. The WHAM[35,36] technique was used to match the individual umbrella windows to obtain a continuous free energy profile. This PMF was then used to construct the initial adaptive potential for the subsequent PMF calculations with an adjustable V_{ii}^0 term for fitting to the experimental pK_a. All other parameters are fixed to their optimized gas phase values at this stage of the parametrization. During the adaptive simulations, the restraining potential applied to the CEC corresponds to the relevant ξ_{CEC} range of the previously calculated PMF, which was then multiplied by -1 and harmonically capped at each end. The windows were equilibrated for 25 ps, and then data was collected in a constant NVT ensemble[41] using a Nose-Hoover thermostat for a simulation time of 100 ps to 1 ns, depending on the window convergence. A total of 5 to 15 adaptive windows were used, spanning the range $\xi_0^n = 0.68$ to 6.55 Å.

D. Simulation Details for Glutamic Acid. The gas phase cluster model for glutamic acid includes 5 solvating waters and an all-atom representation of the protonated glutamic acid

MS-EVB Description of Protonatable Amino Acids

J. Phys. Chem. A, Vol. 110, No. 2, 2006 **635**

residue that is terminated by standard AMBER[29] capping residues Ace and Nme. All QM calculations were performed using the *Gaussian 03* program package[37] at the level of DFT using the B3LYP/6-31G(d,p) functional/basis set. For the calculation of the ab initio PES, a series of relaxed PT scans were performed whereby the geometries of the cluster were optimized as a parametric function of the donor−acceptor separation ($R_{O_\gamma O}$ = 2.3, 2.4, 2.5, 2.6, 2.7, 2.8, 2.9 Å) and the donor−proton bond length. The equilibrium bond lengths ($R_{O_\gamma O}$ and $R_{O_\gamma H^+}$) and equilibrium bond angle ($\angle_{O_\gamma H^+ O}$) were also included in the target function for the Simplex[30] optimization of the MS-EVB parameters. For the MS-EVB calculations, the partial charges of the protonated glutamic acid residue GluH were derived using the RESP[42] method from a DFT calculation at the level of B3LYP/6311++G(2d,p) functional/basis set. Except for the Morse potential accounting for the dissociation limit of the $O_\gamma H^+$ bond in the GluH residue, all interactions for the model Ace-GluH-Nme molecule were described within the AMBER[29] force field. The Morse parameters obtained from fitting the functional form to the QM gas phase dissociation potential energy profile are a_0 = 143.48 kcal/mol, a_1 = 1.98 Å^{-1}, and a_2 = 0.99 Å.

The solution phase glutamic acid model consists of the above Ace/Nme-terminated glutamic acid residue immersed in an orthorhombic simulation cell (31.37 × 31.18 × 31.24 Å³) containing 998 modified TIP3P water molecules. The AMBER[29] force field with the modifications noted above was used to describe the amino acid model. Periodic boundary conditions were employed, and the long-range Coulombic interactions were treated with particle mesh Ewald.[40] The short-range nonbonded interactions and forces were subject to a 13.0 Å cutoff. The MD time integration step within the Verlet integrator was 0.5 fs. Prior to the MS-EVB production run, the classical system was equilibrated for 4 ns in the constant NPT ensemble and then another 2 ns in the constant NVT ensemble.[41]

For the calculation of the PMF, a series of 30 umbrella windows were used to restrain the sampling of ξ_{CEC} over the range 0.8−6.6 Å. Each window was equilibrated for 100 ps in the constant NVT ensemble[41] using a Nose-Hoover thermostat followed by 500 ps of data collection. The WHAM[35,36] technique was used to unbias and combine the sampling from all the windows to form the free energy profile corresponding to evolution on the MS-EVB ground state surface. Using eq 9, the pK_a was computed and the iterative procedure described in section 2B was then used to self-consistently determine a final set of MS-EVB parameters.

3. Results and Discussion

A. MS-EVB Parameters and Equilibrium Geometries. The results of the MS-EVB models for the ionizable histidine and glutamic acid residues are given in Table 1. For histidine, all the adjustable parameters were initially fit to reproduce ab initio energetics and equilibrium geometric features of the HisH$^+$−(H$_2$O)$_3$ cluster in the gas phase. Keeping all other parameters constrained to their optimized values from the cluster parametrization, the constant energy correction V_{ii}^0 (of the protonated histidine EVB state relative to the hydronium EVB state) was then adjusted to reproduce the experimental equilibrium concentrations for the aqueous phase dissociation reaction. A value of −97.90 kcal/mol provided a simulation pK_a of 6.3 is in good agreement with the experimental value of 6.04 to 6.07. The above procedure constitutes one iteration step within the self-consistent determination of the MS-EVB parameters for glutamic acid. Once we have determined a V_{ii}^0 that gives the correct

TABLE 1: MS-EVB Parameters for the Histidine and Glutamic Acid Residues

parameter	histidine	glutamic acid
V_{ii}^0	−97.90 kcal mol^{-1}	−106.72 kcal mol^{-1}
V_{ij}^{const}	−96.92 kcal mol^{-1}	−26.43 kcal mol^{-1}
r_{sc}^0	1.19 Å	1.03 Å
λ	0.06	−0.076
R_{DA}^0	2.47 Å	2.57 Å
C	0.46	0.8911
α	1.33 Å^{-2}	1.83 Å^{-2}
a_{DA}	3.72 Å	2.86 Å
β	3.50 Å^{-2}	−0.058 Å^{-2}
b_{DA}	2.20 Å	2.27 Å
ϵ	13.54 Å^{-1}	1.77 Å^{-1}
c_{DA}	2.25 Å	2.59 Å
γ	2.27 Å^{-2}	6.43 Å^{-2}

dissociation reaction in solution, all other parameters are reoptimized to reproduce the ab initio energetics and equilibrium geometric properties of the GluH−(H$_2$O)$_5$ gas phase cluster. Next, these optimized parameters are constrained and V_{ii}^0 is adjusted to reproduce the experimental pK_a. The above steps are repeated until the optimization has reached self-consistency in the parameter values. Given the measured pK_a of 4.07 for glutamic acid, it was found that the MS-EVB parameters given in Table 1 provide the best agreement with the QM PT PES, QM equilibrium geometric features, and experimental pK_a; the calculated pK_a from simulation is 4.3.

Although the parametrization scheme used for the glutamic acid residue is more involved than the approach selected for histidine, it is not clear which provides better parameters. One advantage of the self-consistent procedure is the possible transferability of the parameters between the gas phase cluster model and the condensed phase system. If the functional forms in the force field are sufficiently flexible, then one can in principle determine a set that is applicable for clusters of arbitrary size by including these systems in the parametrization. However, the additional computational cost required for determining a general parameter set may make this prescription unattractive. Furthermore, when the functions depend nonlinearly on the parameters, as is the case in the MS-EVB force field, the solution is not unique. The possibility of obtaining multiple solutions to the same problem raises the question if it is even worth the effort to seek transferability of the parameters between the cluster model and the bulk system. The critical test of a force field is its capacity to correctly predict the properties of related systems that were not explicitly included within the parametrization set. The performance in protein simulations will be the key test for the histidine and glutamic acid MS-EVB models.

To assess the accuracy of the MS-EVB potential, we compare the equilibrium geometric properties to those obtained from ab initio calculations. The QM results are from a DFT geometry optimization of the amino acid−water cluster using the B3LYP/6-31G(d,p) functional/basis set. Density functional theory was chosen because electron correlation has a noticeable effect on the optimized geometry of the PT systems.[43] The MS-EVB results are from a simulated annealing to zero temperature trajectory. For a proton transfer reaction, the important geometric elements are the donor−acceptor distance R_{DA}, the donor-proton distance R_{DH^+}, and the angle $\angle_{DH^+A}$ formed by the proton with the donor and acceptor. Table 2 shows that the MS-EVB force field is capable of reproducing the important equilibrium bond lengths. The histidine model provides better agreement with the B3LYP hydrogen bond angle geometry than the glutamic acid

TABLE 2: Comparison of Equilibrium Geometric Properties

property	system	EVB	B3LYP[a]
R_{DH^+}	$HisH^+-(H_2O)_3$	1.06 Å	1.07 Å
	$GluH-(H_2O)_5$	1.06 Å	1.06 Å
R_{DA}	$HisH^+-(H_2O)_3$	2.69 Å	2.62 Å
	$GluH-(H_2O)_5$	2.53 Å	2.48 Å
$\angle_{DH^+A}$	$HisH^+-(H_2O)_3$	167.9°	165.0°
	$GluH-(H_2O)_5$	179.9°	173.3°

[a] Calculation was performed using the 6-31G(d,p) basis set.

TABLE 3: Hydrogen Bonding Energies of $HisH^+-(H_2O)_n$[a] Clusters

	EVB	HF[b]	B3LYP[b]
$HisH^+-H_2O$	−18.56	−17.20	−17.35
$HisH^+-(H_2O)_2$	−38.01	−26.64	−32.22
$HisH^+-(H_2O)_3$	−49.32	−42.13	−45.50

[a] All energies are reported in units of kcal/mol. [b] Calculations were performed using the 6-31G(d,p) basis set.

model. Since the angle of the glutamic acid−water complex is within the range of what is considered a hydrogen bond in conventional MD, the small deviation from the QM optimized geometry is not expected to impact the performance of the model. The overall agreement in the comparison for the two models indicates that the MS-EVB force field is adequate in reproducing key equilibrium geometries.

To investigate the capacity of the force field in reproducing solvation effects, we compute the hydrogen bonding energies as a function of the water cluster size. Table 3 compares the total hydrogen bonding energies obtained from the EVB, Hartree−Fock (HF), and DFT approaches for the $HisH^+-$ $(H_2O)_n$ (n = 1, 2, or 3) clusters. We define the total hydrogen bonding energy as the difference between the energies of the amino acid−water cluster and the bare gas phase amino acid. The energies from the QM calculations correspond to the equilibrium energies (geometry-optimized clusters), while the EVB energies correspond to cluster configurations obtained from simulated annealing to zero temperature trajectories. The MS-EVB model provides hydrogen bonding energies that are closer to B3LYP than HF; however, the model consistently overestimates the energies when compared to B3LYP, which may cause a slight overstabilization of the solvated structures during the simulations. Given that DFT methods include some measure of electronic correlation, which has been shown to be important for describing hydrogen bonding interactions, it is encouraging that the MS-EVB force field gives results that are in reasonable agreement with the much more computationally expensive QM approach.

B. Amino Acid Free Energy of Deprotonation. The PMF for the protonation/deprotonation reaction provides information about the relative stability of the reactant and product states as well as the height of the transition state barrier that separates them. The present choice for the RC ξ_{CEC} is the position of the CEC relative to the donor atom of the amino acid residue. Thus, at low values of ξ_{CEC}, the system corresponds to the undissociated acid molecule solvated in water; whereas, for large ξ_{CEC}, the system corresponds to the solvent-separated conjugate base of the amino acid and the hydronium cation. The black curves in Figure 2 show the PMF $W(\xi_{CEC})$ for the (A) histidine and (B) glutamic acid dissociation reactions.

The free energy (FE) curve gives a PT barrier for histidine deprotonation and histidine protonation of 10.38 and 1.39 kcal/mol, respectively. The free energy of reaction for deprotonation is 9.2 kcal/mol, which agrees reasonably well with the experi-
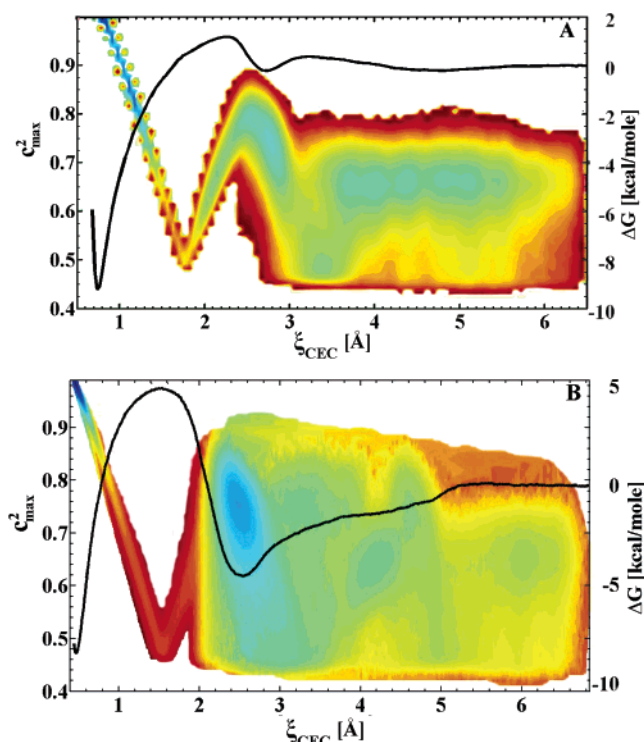

Figure 2. Free energy profiles for the amino acid deprotonation reaction (black curve). 3-D plot of the deprotonation free energy surface as a function of the center of excess charge coordinate ξ_{CEC} and the largest EVB state population c_{max}^2 (colored contours). (A) Histidine. (B) Glutamic acid.

mental reaction free energy of 8.29 to 8.33 kcal/mol, estimated from the equation

$$\Delta G = 2.3RT(pK_a) \tag{14}$$

where R denotes the molar gas constant, T represents the standard temperature, and the pK_a has been experimentally measured to be between 6.04 and 6.07 units for histidine in bulk water. In Figure 2A, the first minimum of the FE curve corresponds to the protonated histidine species, while the second shallow minimum corresponds to a local stabilized environment where the excess proton resides on the first solvating water. The third minimum (plateau) is due to the solvent stabilization of the excess proton charge. The solvent stabilization of the excess proton in bulk is clearly evident beyond 4.5 Å. Since the PMF that enters in the calculation of the pK_a is zeroed with respect to the free energy of the hydronium in the bulk [see eq 9 and Supporting Information], it is important to sample the CEC many angstroms away from the weak acid. If the FE curve is stopped prematurely, the resulting free energy of reaction (solvation) will not be calculated from bulk properties but from an intermediate structured environment, thereby leading to an incorrect pK_a.

The FE curve in Figure 2B gives a PT barrier for glutamic acid deprotonation and glutamate protonation of 13.02 and 8.55 kcal/mol, respectively. The difference in the free energies between the solvated glutamic acid (first minimum) and the solvent separated glutamate and hydronium cation (bulk limit of the PMF) is approximately 8 kcal/mol, which does not agree as well with the experimental estimate of 5.5 kcal/mol using eq 14. This discrepancy may be due to the fact that the difference of two PMF values does not rigorously correspond to the FE difference. In constructing the PMF, the RC degree of freedom is projected out of the phase space integration; whereas the
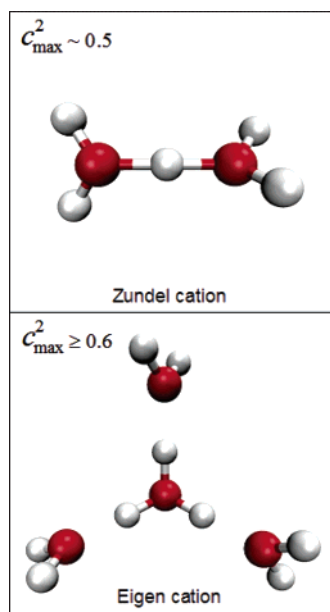
MS-EVB Description of Protonatable Amino Acids

J. Phys. Chem. A, Vol. 110, No. 2, 2006 **637**

Figure 3. Structure of the water Zundel and Eigen cations. The Zundel and Eigen cations correspond to the largest EVB state population c_{max}^2 of ~0.5 and ≥0.6, respectively.

partition function (which gives FEs) entails integration over all phase space. Equation 9 provides a rigorous approach within classical statistical mechanics for computing the pK_a from simulation data, which is the quantity one should compare with experiment. The procedure entails integration over the RC degree of freedom that was projected out in the PMF.

While ξ_{CEC} is a natural RC for monitoring the progress of the deprotonation reaction, it does not provide any information about the structure of the hydronium cation, i.e., whether the hydronium is an Eigen or a Zundel complex. It has been shown numerically, within the MS-EVB approach, that the range of value of the largest EVB state population c_{max}^2 uniquely characterizes the solvation structure of the excess proton. An EVB state population greater than 0.6 delineates the Eigen cation, while a value around 0.5 characterizes the Zundel. Schematic representations of these two complexes are shown in Figure 3.

To better understand the nature of the hydronium complex during the deprotonation process, it is meaningful to represent the PMF as a function of ξ_{CEC} as well as the largest EVB state population c_{max}^2. This two-dimensional (2-D) PMF, $W(\xi_{CEC}, c_{max}^2)$, can be constructed using the equation

$$W(\xi_{CEC}, c_{max}^2) = W(\xi_{CEC}) - k_B T \ln\langle\rho(c_{max}^2; \xi_{CEC})\rangle + C \tag{15}$$

where $W(\xi_{CEC})$ is the 1-D PMF depicted by the black curves in Figure 2, $\langle\rho(c_{max}^2; \xi_{CEC})\rangle$ is the average density of c_{max}^2 at a given ξ_{CEC}, and C is a constant.[44] Figure 2 shows the 2-D PMF contours as a function of ξ_{CEC} and c_{max}^2 for (A) histidine and (B) glutamic acid.

At short distances, HisH[+] is the most stable form with the corresponding EVB amplitude over 90%. As the reaction coordinate increases, the CEC becomes delocalized over the His and the first solvating water. At around 1.8 Å a Zundel structure is formed between the His and the first solvating water. Increasing the reaction coordinate further causes the CEC to first become localized predominantly on the first solvated water and then become delocalized, forming a $H_5O_2^+$ Zundel cation at 3.4 Å. After 3.4 Å the CEC forms an Eigen cation while it

diffuses through the solvent, in agreement with our previous simulations of the excess proton in bulk water.[26] The 2-D PMF monitors the progress of the PT event, while also elucidating the characteristics of the structures formed during the reaction. A comparison of the 1-D PMF (black curve) and the 2-D contours in Figure 2A shows that the local minimum at 2.5 Å in the PMF corresponds to the proton on the first solvating water in its Eigen cation form. The local minimum is more stable than the solvent stabilized Eigen cation by 0.21 kcal/mol. This can be explained by the formation of the strong hydrogen bond between histidine and the Eigen cation. The energy stabilization can be attributed to one of the Eigen cation's hydrogen bonds with a surrounding water molecules being replaced by a stronger hydrogen bond with the nitrogen of the deprotonated histidine.

The colored contours in Figure 2B indicates that the first miminum corresponds to the glutamic acid GluH, where this EVB state contributes approximately 99% of the population to the ground state. Near the transition state region at $\xi_{CEC} = 1.5$ Å, the hydronium complex assumes the Zundel form where the excess proton is shared between the amino acid and the first solvation water. An Eigen cation is formed at the second minimum and is stabilized by the glutamate anion Glu[−]. This charge stabilization accounts for approximately 4.5 kcal/mol relative to the solvent stabilized Eigen in the bulk. It is not until the Eigen diffuses beyond the second solvation shell ($\xi_{CEC} > 5$ Å) that the interactions of the solvent separated ion pairs become attenuated sufficiently to give rise to bulk features in the PMF.

C. Solvation Structure. A useful aspect of MS-EVB simulation is the ability to evaluate the solvation structure during the PT event. The solvation structure can be characterized by the radial distribution function (RDF). The RDFs for the $N_\delta O$, $N_\delta H$, and $N_\delta Cl^-$ atom pairs in the histidine system are shown in Figure 4. As one can see from the $N_\delta O$ RDF (Figure 4A), the oxygen atom of the water molecule in the first solvation shell stays at about 2.65 Å from the protonated nitrogen atom of the histidine, and this distance increases to 2.85 Å as dissociation progresses along the reaction coordinate (at large ξ_{CEC}). The amplitude of the first peak and the minimum following the first peak show that the first solvating water associates very strongly as the proton is transferred from HisH[+] to the first water. When the first protonated water is in its Eigen cation form at around 2.5 Å, there is a reduction in the amplitude of the first peak and density begins to accumulate in the first minimum. This indicates that the Eigen cation is not strongly bound to the His molecule and that the hydronium ion is becoming more mobile. In the Zundel water structure that follows the Eigen cation formation, the amplitude of the first peak in the corresponding cross section of the RDF decreases significantly while the first minimum is almost nonexistent. This is due to the formation of a strong hydrogen bond between the water molecules in the first and second solvation shells. At further dissociation, the first peak stabilizes at a moderate intensity representing the transient hydrogen bond of the first solvating water with a His molecule. The second peak in the RDF of the $N_\delta O$ pair exhibits very dynamical behavior with increasing ξ_{CEC}. It is clear that as the ξ_{CEC} increases, the predominant second water peak draws closer to the first peak until they merge at the water–water Zundel structure and then the second water returns to a position farther away form the first water at large ξ_{CEC}. The $N_\delta H$ RDF (Figure 4B) shows the same basic trends seen in the $N_\delta O$ RDF with the exception that the shift of the first peak from a short distance to larger distance is more pronounced. This is accounted for because the position
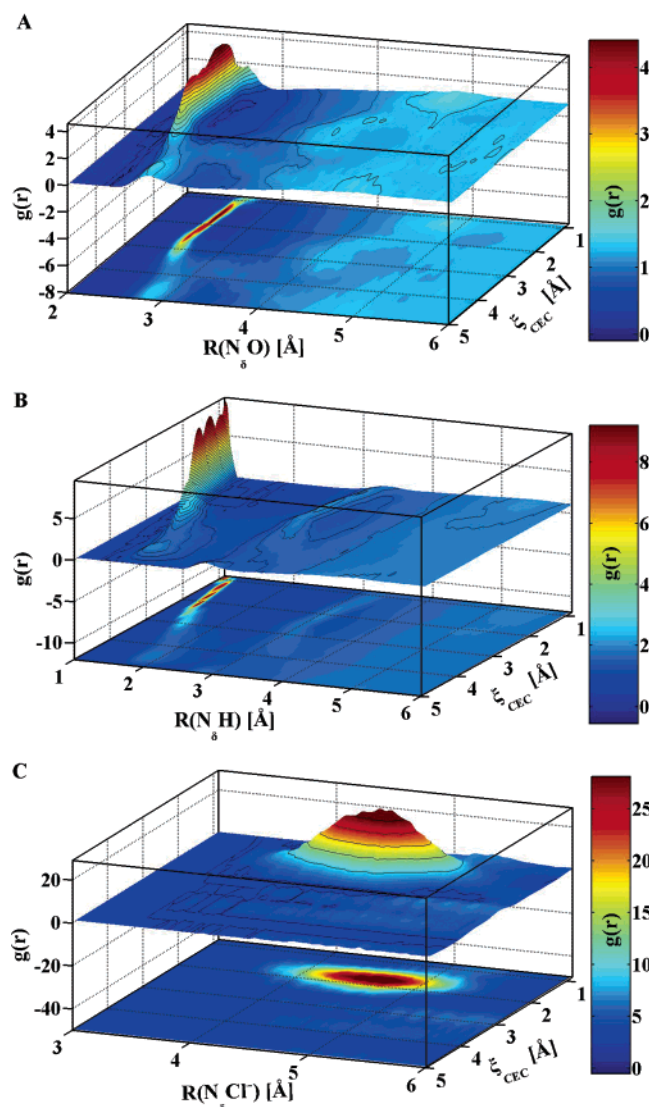
Figure 4. 2-D radial distribution function: (A) $g_{N_\delta O}(r;\xi_{CEC})$, (B) $g_{N_\delta H}(r;\xi_{CEC})$, and (C) $g_{N_\delta Cl^-}(r;\xi_{CEC})$.

of the excess charge skews the data at small ξ_{CEC} where it is the closest hydrogen to the His molecule.

The surprising result is the position of the counterion during the deprotonation process (Figure 4C). It is striking that the chloride ion is freely diffusing at small and large values of ξ_{CEC}, yet when the first water forms a Zundel-like cation with histidine, the chloride strongly associates with the complex to form a contact ion pair. This complex seems to be close to the maximum value, transition state, of the PMF.

The solvation structures shown in Figure 5 for the glutamic acid model exhibit features similar to those of the histidine. Panel A displays the RDF between the O_γ of the glutamic acid and the water oxygens. As the acid dissociates, the first solvation water, which is approximately 2.5 Å away, approaches to accept the excess proton. This distance increases to about 2.75 Å as the hydronium cation diffuses into the bulk. The first peak of the $O_\gamma H$ RDF (Figure 5B) shows a trend simlar to that observed in histidine of increasing in distance along the deprotonation RC, while at small values of ξ_{CEC}, the excess proton contributes a significant percentage to the RDF. This combined with the restricted mobility in the PMF wells gives rise to the higher intensity peak compared to the bulk environment.
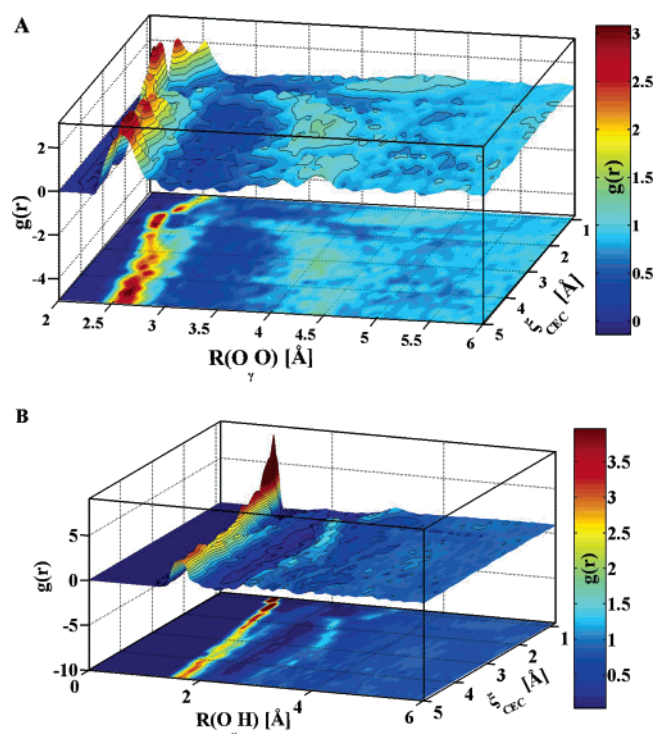

Figure 5. 2-D radial distribution function: (A) $g_{O_\gamma O}(r;\xi_{CEC})$ and (B) $g_{O_\gamma H}(r;\xi_{CEC})$.

4. Conclusions

This paper has presented the development of the MS-EVB force field for describing the aqueous phase deprotonation of amino acids, specifically histidine and glutamic acid. Fitting of the parameters to reproduce relevant ab initio equilibrium geometric properties and the PT PES for small amino acid−water clusters in the gas phase provided an initial model, which was then optimized to reproduce experimental pK_a measurements. Importantly, this force field includes the effects of the Grotthuss proton shuttling and delocalization in the acid ionization process, which has not before been included in such molecular models. The MS-EVB model for amino acids consists of a modified AMBER[29] force field for the descriptions of the EVB states and functional forms and associated parameters for the description of the couplings among these states. In this prescription, the system evolves on the ground state of the MS-EVB Hamiltonian expressed in the representation of empirically determined valence bond states.

Molecular dynamics simulations of histidine and glutamic acid dissociation in the aqueous environment have illustrated fundamental elements of the PT dynamics. During the initial events, the excess proton CEC moves from being completely localized on the amino acid molecule to forming a Zundel cation with the closest solvating water. At the next stage, an Eigen cation is formed in the first solvation shell and is stabilized by a pair of hydrogen bonding waters and the deprotonated amino acid. In the histidine system, this stabilization is a hydrogen bonding interaction (between the N_δ of the imidazole moiety and a hydronium proton); whereas for the glutamic acid case, this stabilization is electrostatic in nature (between the newly formed glutamate/hydronium contact ion pairs). In the final stage, a water−water Zundel cation is formed which then is transformed into the solvent-stabilized Eigen cation in the bulk.

While these key steps of the solution phase PT dynamics are interesting, our motivation for developing protonatable amino acid models is for the elucidation of important PT pathways in

MS-EVB Description of Protonatable Amino Acids

J. Phys. Chem. A, Vol. 110, No. 2, 2006 **639**

biological systems. The parametrization described herein provides the framework for the modeling of, for example, the HCA enzyme and the M2 channel with explicit dissociable histidine residues, which have been implicated in experiments as being critical for the PT mechanism. Future studies will also explore the effects of mutations (for example, mutating the His64 in HCA to Glu64) on PT. The incorporation of the histidine and glutamic acid models into these protein environments will be the ultimate test of the MS-EVB force field in describing dynamical and structural data during the PT events and in predicting intrinsic pK_a values in the protein environment. The systematic parametrization scheme presented here allows for the inclusion of other protonatable amino acids, which may be crucial in the context of protein engineering.

Supporting Information Available: An appendix detailing the derivation of eq 9. This material is available free of charge via the Internet at http://pubs.acs.org.

References and Notes

(1) Warshel, A. *Computer Modeling of Chemical Reactions in Enzymes and Solutions*; John Wiley and Sons: New York, 1991.

(2) Pinto, L. H.; Holsinger, L. J.; Lamb, R. A. *Cell* **1992**, *69*, 517.

(3) Wang, C.; Lamb, R. A.; Pinto, L. H. *Biophys. J.* **1995**, *69*, 1363.

(4) Steiner, H.; Jonsson, B.-H.; Lindskog, S. J. *Eur. J. Biochem.* **1975**, *59*, 253.

(5) Jonsson, B.-H.; Steiner, H.; Lindskog, S. *FEBS Lett.* **1976**, *64*, 310.

(6) Silverman, D. N.; Vincent, S. H. *Crit. Rev. Biochem.* **1983**, *14*, 207.

(7) Silverman, D. N.; Lindskog, S. *Acc. Chem. Res.* **1988**, *21*, 30.

(8) Eriksson, A. E.; Jones, A. T.; Liljas, A. *Proteins* **1988**, *4*, 274.

(9) Tu, C.; Silverman, D. N.; Forsman, C.; Jonsson, B.-H.; Lindskog, S. *Biochemistry* **1989**, *28*, 7913.

(10) Lindskog, S.; Behravean, G.; Engstrant, C.; Forsman, C.; Jonsson, B.; Liang, Z.; Ren, X.; Xue, Y. In *Carbonic Anhydrase: From Biochemistry and Genetics to Physiology and Clinical Medicine*; Lindskog, S., Behraven, G., Engstrant, C., Forsman, C., Jonsson, B., Liang, Z., Ren, X., Xue, Y., Eds.; Weinheim, 1991; p 1.

(11) Håkansson, K.; Carlsson, M.; Svensson, L. A.; Liljas, A. *J. Mol. Biol.* **1992**, *227*, 1192.

(12) Christianson, D. W.; Fierke, C. A. *Acc. Chem. Res.* **1996**, *29*, 331.

(13) Lindskog, S. *Pharmacol. Ther.* **1997**, *74*, 1.

(14) Toba, S.; Colombo, G.; Merz, K. M., Jr. *J. Am. Chem. Soc.* **1999**, *121*, 2290.

(15) Fisher, Z.; Hernandez, Prada, J. A.; Tu, C.; Duda, D.; Yoshioka, C.; An, H.; Govindasamy, L.; Silverman, D. N.; McKenna, R. *Biochemistry* **2005**, *44*, 1097.

(16) Jordan, F. *Science* **2004**, *306*, 818.

(17) Frank, R. A. W.; Titman, C. M.; Pratap, J. V.; Luisi, B. F.; Perham, R. N. *Science* **2004**, *306*, 872.

(18) Qian, M.; Tu, C.; Earnhardt, N.; Laipis, P. J.; Silverman, D. N. *Biochemistry* **1997**, *36*, 15758.

(19) An, H.; Tu, C.; Duda, D.; Montanez-Clemente, I.; Math, K.; Laipis, P. J.; McKenna, R.; Silverman, D. N. *Biochemistry* **2002**, *41*, 3235.

(20) Duda, D.; Tu, C.; Qian, M.; Laipis, P.; Agvandje-McKenna, A.; Silverman, D. N.; McKenna, R. *Biochemistry* **2001**, *40*, 1741.

(21) Danneel, H. Z. *Elektrochem. Angew. Phys. Chem.* **1905**, *11*, 249.

(22) de Grotthus, C. J. T. *Ann. Chim. (Cachan, Fr.)* **1806**, *58*, 54.

(23) Schmitt, U. W.; Voth, G. A. *J. Phys. Chem. B.* **1998**, *102*, 5548.

(24) Schmitt, U. W.; Voth, G. A. *J. Chem. Phys.* **1999**, *111*, 9361.

(25) Schmitt, U. W.; Voth, G. A. *Isr. J. Chem.* **1999**, *39*, 483.

(26) Day, T. J.; Soudackov, A. V.; Cuma, M.; Schmitt, U. W.; Voth, G. A. *J. Chem. Phys.* **2002**, *117*, 5839.

(27) Cuma, M.; Schmitt, U. W.; Voth, G. A. *Chem. Phys.* **2000**, *258*, 187.

(28) Cuma, M.; Schmitt, U. W.; Voth, G. A. *J. Phys. Chem. A* **2001**, *105*, 2814.

(29) Cornell, W. D.; Cieplak, P.; Bayly, C. I.; Gould, I. R.; Merz, K. M., Jr.; Ferguson, D. M.; Spellmeyer, D. C.; Fox, T.; Caldwell, J. W.; Kollman, P. A. *J. Am. Chem. Soc.* **1995**, *117*, 5179.

(30) Rowan, T. *Functional Stability Analysis of Numerical Algorithms*; University of Texas: 1990.

(31) Chandler, D. *Introduction to Modern Statistical Mechanics*; Oxford University Press: New York, 1987.

(32) Patey, G. N.; Valeau. *J. Chem. Phys.* **1975**, *63*, 2334.

(33) Pangali, C.; Rao, M.; Berne, B. J. *J. Chem. Phys.* **1979**, *71*, 2975.

(34) Mezei, M. *J. Comput. Phys.* **1987**, *68*, 237.

(35) Kumar, S.; Bouzida, D.; Swendsen, R. H.; Kollman, P. A.; Rosenberg, J. M. *J. Comput. Chem.* **1992**, *13*, 1011.

(36) Roux, B. *Comput. Phys. Commun.* **1995**, *91*, 275.

(37) Frisch, M. J.; Trucks, G. W.; Schlegel, H. B.; Scuseria, G. E.; Robb, M. A.; Cheeseman, J. R.; Montgomery, J. A., Jr.; Vreven, T.; Kudin, K. N.; Burant, J. C.; Millam, J. M.; Iyengar, S. S.; Tomasi, J.; Barone, V.; Mennucci, B.; Cossi, M.; Scalmani, G.; Rega, N.; Petersson, G. A.; Nakatsuji, H.; Hada, M.; Ehara, M.; Toyota, K.; Fukuda, R.; Hasegawa, J.; Ishida, M.; Nakajima, T.; Honda, Y.; Kitao, O.; Nakai, H.; Klene, M.; Li, X.; Knox, J. E.; Hratchian, H. P.; Cross, J. B.; Adamo, C.; Jaramillo, J.; Gomperts, R.; Stratmann, R. E.; Yazyev, O.; Austin, A. J.; Cammi, R.; Pmelli, C.; Ochterski, J. W.; Ayala, P. Y.; Morokuma, K.; Voth, G. A.; Salvador, P.; Dannenberg, J. J.; Zakrzewski, V. G.; Dapprich, S.; Daniels, A. D.; Strain, M. C.; Farkas, O.; Malick, D. K.; Rabuck, A. D.; Raghavachari, K.; Foresman, J. B.; Ortiz, J. V.; Cui, Q.; Baboul, A. G.; Clifford, S.; Cioslowski, J.; Stefanov, B. B.; Liu, G.; Lianshenko, A.; Piskorz, P.; Komaromi, I.; Matin, R. L.; Fox, D. J.; Keith, T.; Al-Laham, M. A.; Peng, C. Y.; Nanyakkara, A.; Chalacombe, M.; Gill, P. M. W.; Johnson, B.; Chen, W.; Wong, M. W.; Gonzalez, C.; Pople, J. A. *Gaussian 03*; revision B.02; Gaussian Inc.: Pittsburgh, PA, 2003.

(38) Smith, W.; Forester, T. R. *The DL_POLY_2 User Manual*; CCLRC, Daresbury Laboratory: Daresbury, Warrington, England, 1999.

(39) Smondyrev, A. M.; Voth, G. A. *Biophys. J.* **2002**, *82*, 1460.

(40) Hummer, G.; Pratt, L. R.; Garcia, A. E. *J. Phys. Chem.* **1996**, *100*, 1206.

(41) Kast, S. M.; Nicklas, K.; Bär, H.-J.; Brickmann, J. *J. Chem. Phys.* **1994**, *100*, 566.

(42) Cieplak, P.; Cornell, W. D.; Bayly, C.; Kollman, P. A. *J. Comput. Chem.* **1995**, *16*, 1357.

(43) Nagy, P. I.; Durant, G. J.; Smith, D. A. *J. Am. Chem. Soc.* **1993**, *115*, 2912.

(44) Allen, T. W.; Andersen, O. S.; Roux, B. *Proc. Natl. Acad. Sci. U.S.A.* **2004**, *101*, 117.